THE EUROPEAN PHYSICAL JOURNAL C

Exact cosmological models in metric-affine $F(R, T)$ gravity

Dinesh Chandra Maurya[1,a] **, Ratbay Myrzakulov**[2,b]

[1] Centre for Cosmology, Astrophysics and Space Science, GLA University, Mathura, Uttar Pradesh 281 406, India
[2] Department of General and Theoretical Physics, Eurasian International Centre for Theoretical Physics, Eurasian National University, 010008 Astana, Kazakhstan

Abstract A flat Friedmann–Lematre–Robertson–Walker (FLRW) spacetime metric was used to investigate some exact cosmological models in metric-affine $F(R, T)$ gravity in this paper. The considered modified Lagrangian function is $F(R, T) = R + \lambda T$, where R is the Ricci curvature scalar, T is the torsion scalar for the non-special connection, and λ is a model parameter. We also wrote $R = R^{(LC)} + u$ and $T = T^{(W)} + v$, where $R^{(LC)}$ is the Ricci scalar curvature with respect to the Levi–Civita connection and $T^{(W)}$ is the torsion scalar with respect to the Weitzenbock connection, and u and v are the functions of scale factor $a(t)$, connection and its derivatives. For the scale factor $a(t)$, we have obtained two exact solutions of modified field equations in two different situations of u and v. Using this scale factor, we have obtained various geometrical parameters to investigate the universe's cosmological properties. We used Markov chain Monte Carlo (MCMC) simulation to analyze two types of latest datasets: cosmic chronometer (CC) data (Hubble data) points and Pantheon SNe Ia samples, and found the model parameters that fit the observations best at $1 - \sigma$, and $2 - \sigma$ regions. We have performed a comparative and relativistic study of geometrical and cosmological parameters. In model-I, we have found that the effective equation of state (EoS) parameter ω_{eff} varies in the range $-1 \leq \omega_{eff} \leq 0$, while in model-II, it varies as $-1.0345 \leq \omega_{eff} \leq 0$. We found that both models are transit phase (moving from slowing down to speeding up) universes with a transition redshift $z_t = 0.5874^{+0.2130}_{-0.0197}$ and $z_t = 0.6865^{+0.1719}_{-0.0303}$.

Contents

[a] e-mail: dcmaurya563@gmail.com (corresponding author)
[b] e-mail: rmyrzakulov@gmail.com

1 Introduction

Recent cosmological studies [1–7] suggest that the Universe evolves with two accelerating phases of expansion, one at early times and one at late times. Although the latter can be explained by the presence of a cosmological constant Λ, the inclusion of some modification was necessary due to the associated theoretical issue, the potential for dynamical behavior, and particularly the cosmological constant's incapacity to explain the early accelerated phase. One possible approach is to stick with general relativity as the basic theory and change the universe's matter content by adding new fields, like the dark energy sector at later times [8,9] and/or the inflaton at earlier times [10,11]. A second option involves altering the gravitational sector itself, creating a theory that, although having general relativity as a specific limit, generally shows more degrees of freedom [12,13].

A variety of methods construct gravitational modifications, each moderating a different aspect of general relativity. The braneworld theories [14] comes from changing the dimensionality; the $F(R)$ gravity [15,16], $F(G)$ gravity [17,18], Lovelock theories [19,20], etc. come from changing the Einstein-Hilbert Lagrangian; and the Horndeski/Galileon

theories [21–23] come from adding a scalar field coupled in different ways with curvature. It is also possible to make changes using torsional invariants. This can be done in $F(T)$ gravity [24,25], $F(T, T_G)$ gravity [26], or scalar-torsion theories [27,28], starting with the similar teleparallel formulation of gravity [29,30]. Furthermore, we can create a large group of metric-affine theories, each with its own generic linear connection structure [31–33]. On the other hand, nonlinear connections can be added, as seen in Finsler and Finsler-like theories [34–39].

These affinely connected metric theories, and more specifically the Riemann–Cartan subclass of these theories [40], could be used to make a theory with a certain but not unique connection. This would result in both non-zero curvature and non-zero torsion at the same time, providing the additional degrees of freedom usually required in any gravitational modification [41]. As a result, metric-affine gravity can produce a good phenomenology that can explain both the early and late universe evolution [42–46]. A new paper, [42], looks at the cosmology that comes from using this kind of framework and figures out how things that can be seen change over time, like the density parameters and the effective dark energy equation-of-state parameter. Using the mini-superspace technique, they have studied cosmological behavior, focusing on the effect of the connection and expressing the theory as a deformation from both general relativity and its teleparallel counterpart. Reference [47] has investigated the observational restrictions on metric-affine $F(R, T)$-gravity. In [48–54], several metric-affine gravity theories and their applications are covered.

Recently, [55] has investigated observational constraints on some metric-affine gravity models using a wide range of observational datasets. In [56–58], we have investigated some exact solutions in metric-affine gravity theories with observational constraints. Recently, we have investigated some exact cosmological models in different scenarios in various modified gravity theories [59–65]. Recently, [66] have constructed a cosmological model in non-metricity $f(Q)$ gravity using a special connection and statistically analyzed using information criterion AIC, BIC, and DIC to compare its compatibility with ΛCDM model. Recently, using different special affine connections, [67] investigated $f(Q, C)$ gravity cosmology, including non-metricity with boundary terms. Motivated by the above discussions, in this paper, we find some new exact cosmological models in metric-affine gravity.

This paper is organized as follows: Sect. 1 is introductory. Section 2 provides a brief introduction to metric-affine gravity. Section 3 provides field equations and their exact solutions. In Sect. 4, we perform some observational constraints on different parameters using the latest datasets. Section 5 presents a discussion of the results. Section 6 provides the final conclusions.

2 Metric-affine $F(R, T)$ gravity

In the present section, we organize a brief review of metric-affine gravity, also called $F(R, T)$ gravity, with R as curvature and T known as torsion [41,42]. In this gravity, the choice of a non-special connection is the key factor. Specifically, it is established that enforcing a generic connection $\omega^\alpha{}_{\beta\gamma}$ one defines the torsion tensor and the curvature as [26]

$$R^\alpha{}_{\beta ij} = \omega^\alpha{}_{\beta j,i} - \omega^\alpha{}_{\beta i,j} + \omega^\alpha{}_{\gamma i}\omega^\gamma{}_{\beta j} - \omega^\alpha{}_{\gamma j}\omega^\gamma{}_{\beta i} \quad (1)$$

$$T^\alpha{}_{ij} = e^\alpha{}_{j,i} - e^\alpha{}_{i,j} + \omega^\alpha{}_{\beta i}e^\beta{}_j - \omega^\alpha{}_{\beta j}e^\beta{}_i \quad (2)$$

where $e_\alpha{}^i \partial_i$ is the tetrad field associated with the metric through $g_{ij} = \eta_{\alpha\beta}e^\alpha{}_i e^\beta{}_j$, where $\eta_{\alpha\beta} = diag(1, -1, -1, -1)$, where the The Latin and Greek indices represent the coordinate and tangent space, respectively, and the comma indicates differentiation.

There are numerous possibilities for connections. The only connection that provides vanishing torsion is the Levi–Civita $\Gamma_{\alpha\beta\gamma}$. Henceforth, we will refer to the curvature (Riemann) tensor as $R^{(LC)\alpha}{}_{\beta ij} = \Gamma^\alpha{}_{\beta j,i} - \Gamma^\alpha{}_{\beta i,j} + \Gamma^\alpha{}_{\gamma i}\Gamma^\gamma{}_{\beta j} - \Gamma^\alpha{}_{\gamma j}\Gamma^\gamma{}_{\beta i}$. The Weitzenböck connection, on the other hand, can be used to obtain the following: $T^{(W)k}{}_{ij} = W^k{}_{ji} - W^k{}_{ij}$. This connection is curvatureless and produces only torsion. Quantities corresponding to $W^k{}_{ij}$ are denoted by the label "W". The previous information suggests that the associated Ricci scalar for the Levi-Civita connection is

$$R^{(LC)} = \eta^{\alpha\beta}e_\alpha{}^i e_\beta{}^j$$
$$\left[\Gamma^k{}_{ij,k} - \Gamma^k{}_{ik,j} + \Gamma^l{}_{ij}\Gamma^k{}_{kl} - \Gamma^l{}_{ik}\Gamma^k{}_{jl}\right] \quad (3)$$

while the torsion scalar corresponding to the Weitzenböck connection is

$$T^{(W)} = \frac{1}{4}\left(W^{ikj} - W^{ijk}\right)\left(W_{ikj} - W_{ijk}\right)$$
$$+ \frac{1}{2}\left(W^{ikj} - W^{ijk}\right)\left(W_{kij} - W_{kji}\right)$$
$$- \left(W_j{}^{ij} - W_j{}^{ji}\right)\left(W^k{}_{ik} - W^k{}_{ki}\right) \quad (4)$$

The first is utilized in the Lagrangian of general relativity and in all curvature-based modified gravities, such as in $F(R)$ gravity [15], whereas the second is utilized in the Lagrangian of the teleparallel equivalent of general relativity and in all torsion-modified gravities, such as in $F(T)$ gravity [13].

metric-affine gravity uses a non-special connection with simultaneous non-zero curvature and torsion [42]. Since general relativity and its teleparallel counterpart, which both have two degrees of freedom that correspond to the massless graviton, don't have any extra degrees of freedom, the theory that comes out of them will usually have them, even if the Lagrangian that is used is simple. Here, we consider

the action as

$$I = \int d^4x \, e \left[\frac{1}{2\kappa^2} F(R, T) + L_m \right] \tag{5}$$

where the gravitational constant is $\kappa^2 = 8\pi G$, the matter Lagrangian L_m has also been introduced for completeness, and $e = \det(e_i^\alpha) = \sqrt{-g}$. Take note that the arbitrary function $F(R, T)$ has two variables, R and T, which represent the curvature and torsion scalars, respectively, corresponding to the non-special connection employed [26].

$$T = \frac{1}{4} T^{ijk} T_{ijk} + \frac{1}{2} T^{ijk} T_{kji} - T_j{}^{ji} T^k{}_{ki}, \tag{6}$$

$$R = R^{(LC)} + T - 2T_j{}^{ji}{}_{;i} \tag{7}$$

where the covariant differentiation with regard to the Levi-Civita connection is indicated by the symbol (;). So, while R depends on the tetrad and its first derivative as well as the connection and its first derivative, it also depends on the second tetrad derivative because of the final term in (7). In contrast, T depends on the tetrad field, its first derivative, and the connection. Therefore, we can finally write using Eqs. (4), (6), and (7).

$$R = R^{(LC)} + u, \tag{8}$$
$$T = T^{(W)} + v. \tag{9}$$

The scalar u is contingent upon the tetrad, its first and second derivatives, the connection, and its first derivative, whereas the scalar v is contingent upon the tetrad, its first derivative, and the connection.

The numbers u and v quantify the effect of the specific but non-special imposed connection. If this link turns into the Levi–Civita connection, then $u = 0$ and $v = -T^{(W)}$. This makes the above theory the standard $F(R)$ gravity, which, under $F(R) = R$, coincides with general relativity. Conversely, if the connection is the Weitzenböck one, then $v = 0$ and $u = -R^{(LC)}$, and so the theory corresponds with $F(T)$ gravity. For $F(T) = T$, this gravity thus becomes the teleparallel counterpart of general relativity.

3 Field equations and solutions

We put all of this into a cosmological framework and derive the corresponding field equations that govern the evolution of the universe [42]. We consider the FLRW flat Friedmann homogeneous and isotropic geometry spacetime metric.

$$ds^2 = dt^2 - a^2(t)\delta_{\mu\nu}dx^\mu dx^\nu, \tag{10}$$

which is equivalent to the tetrad $e_i^\alpha = diag[1, a(t), a(t), a(t)]$, in which the scale factor is denoted by $a(t)$. In this situation, the torsion and curvature scalars $T^{(W)} = -6\left(\frac{\dot{a}}{a}\right)^2$ and

$R^{(LC)} = 6\left(\frac{\ddot{a}}{a} + \left(\frac{\dot{a}}{a}\right)^2\right)$ are easily found, respectively. We further consider the conventional substitution $L_m = -\rho_m(a)$ [68–70]. Ultimately, in light of the previous conversation regarding the interdependence of u and v, we consistently enforce that $u = u(a, \dot{a}, \ddot{a})$ and $v = v(a, \dot{a})$.

In this work, we aim to investigate the cosmic behavior resulting just from the non-special connection in metric-affine gravity. Since the coupling coefficient of R can be absorbed into κ^2, we remove it. Instead, we concentrate on the simplest case, where the involved arbitrary function is trivial, which is $F(R, T) = R + \lambda T$. Be aware that the Lagrangian does not explicitly take into account a cosmological constant term. The spacetime metric (10) is added to the action (5), and we get $I = \int L dt$ for this Lagrangian selection [55] as

$$L = \frac{3}{\kappa^2}[\lambda + 1]a\dot{a}^2 - \frac{a^3}{2\kappa^2}[u(a, \dot{a}, \ddot{a}) \\ + \lambda v(a, \dot{a})] + a^3 \rho_m(a). \tag{11}$$

Taking the Hamiltonian constraint $H = \dot{a}\left[\frac{\partial L}{\partial a} - \frac{\partial}{\partial t}\frac{\partial L}{\partial \dot{a}}\right] + \ddot{a}\frac{\partial L}{\partial \ddot{a}} - L = 0$ and extracting the equations of motion for $a(t)$, we have the Friedmann equations as [55]

$$3(1 + \lambda)H^2 - \frac{1}{2}[Ha(u_{\dot{a}} + \lambda v_{\dot{a}}) - (u + \lambda v) \\ + au_{\ddot{a}}(\dot{H} - 2H^2)] = \kappa^2 \rho_m \tag{12}$$

$$(1 + \lambda)(2\dot{H} + 3H^2) - \frac{1}{6}[3Ha(u_{\dot{a}} + \lambda v_{\dot{a}}) - 3(u + \lambda v) \\ - a(u_a + \lambda v_a - \dot{u}_{\dot{a}} - \lambda \dot{v}_{\dot{a}}) \\ - 3a(\dot{H} + 3H^2)u_{\ddot{a}} - 6Ha\dot{u}_{\ddot{a}} - a\ddot{u}_{\ddot{a}}] = -\kappa^2 p_m \tag{13}$$

$$\dot{\rho}_m + 3H(\rho_m + p_m) + \frac{1}{2\kappa^2} \\ \times [\dot{a}(u_a + \lambda v_a) - (\dot{u} + \lambda \dot{v}) + \ddot{a}(u_{\dot{a}} + \lambda v_{\dot{a}}) \\ + (3\dot{a}\dot{H} + \dot{a}H^2 + a\ddot{H})u_{\ddot{a}} \\ + (6\dot{a}H + a\dot{H} - 2aH^2)\dot{u}_{\ddot{a}} + \dot{a}\ddot{u}_{\ddot{a}}] = 0 \tag{14}$$

where H is the Hubble parameter defined by $H = \frac{\dot{a}}{a}$, p_m denotes the matter pressure, and the subscripts $a, \dot{a}, \ddot{a}$ indicate the partial derivatives with respect to these arguments.

We now find the solution to the above field equations for two different choices of u and v, which we investigate in the next two sub-sections. As per definitions of u and v, in the first model, we choose $u = k_1 H - k_2$, $v = k_3 a H - k_4$, and in the second model, we consider $u = k_1(\dot{H} + H^2) - k_2$, $v = k_3 a H - k_4$ with k_i's $i = 1, 2, 3, 4$ constants.

3.1 Model-I

In this model, we choose $u = k_1 H - k_2$ and $v = k_3 a H - k_4$ with k_i's $i = 1, 2, 3, 4$ constants and $H = \frac{\dot{a}}{a}$, then the above

field Eqs. (12) and (13) become

$$3(1+\lambda)H^2 - \frac{1}{2}(k_2 + \lambda k_4) = \kappa^2 \rho_m \tag{15}$$

$$(1+\lambda)(2\dot{H} + 3H^2) - \frac{1}{2}(k_2 + \lambda k_4) = -\kappa^2 p_m \tag{16}$$

$$\dot{\rho}_m + 3H(\rho_m + p_m) = 0 \tag{17}$$

Taking the non-relativistic matter pressure $p_m \approx 0$ in (16) and rewriting the Eq. (16) as

$$2\frac{\ddot{a}}{a} + \left(\frac{\dot{a}}{a}\right)^2 - \frac{k_2 + \lambda k_4}{2(1+\lambda)} = 0, \quad \lambda \neq -1. \tag{18}$$

Solving Eq. (18) for the scale factor $a(t)$, we get

$$a(t) = \left[\frac{3\sqrt{3}c_2 e^{\frac{\sqrt{3n_1}}{2}t} - \sqrt{3}c_1 e^{-\frac{\sqrt{3n_1}}{2}t}}{6\sqrt{n_1}}\right]^{\frac{2}{3}}, \quad n_1 > 0, \tag{19}$$

where c_1, c_2 are arbitrary constants and $n_1 = \frac{k_2 + \lambda k_4}{2(1+\lambda)}$, $\lambda \neq -1$. Without loss of generality, we choose $c_1 = k\sqrt{3}$, $c_2 = \frac{k}{\sqrt{3}}$ so that we can put the scale factor in the following simplified form (hyperbolic expansion law cosmology).

$$a(t) = \left[\frac{k}{\sqrt{n_1}}\sinh\left(\frac{\sqrt{3n_1}}{2}t\right)\right]^{\frac{2}{3}}, \quad n_1 > 0 \tag{20}$$

Alternatively, if we choose $c_1 = 0$, then we find the exponential expansion law cosmology as $a(t) = \frac{\sqrt{3}c_2}{2\sqrt{n_1}}e^{\sqrt{\frac{n_1}{3}}t}$ which gives a constant deceleration parameter q that reveals either a decelerating or accelerating expanding universe, but we seek a transit phase (decelerating-accelerating) expanding

universe model. To investigate the model, we consider the first choice of c_1, c_2. Using the scale factor from (20), we found the Hubble parameter ($H = \frac{\dot{a}}{a}$) and the deceleration parameter ($q = -\frac{a\ddot{a}}{\dot{a}^2}$), which are

$$H(t) = \sqrt{\frac{n_1}{3}}\coth\left(\frac{\sqrt{3n_1}}{2}t\right), \tag{21}$$

$$q(t) = -1 + \frac{3}{2}sech^2\left(\frac{\sqrt{3n_1}}{2}t\right). \tag{22}$$

Now we use the relationship $a(t) = a_0(1+z)^{-1}$ [8], in (21), (22), with the present value of scale factor $a_0 = 1$ in standard convention and z as the redshift, whose positive values show the early evolution of the universe while the negative values of z reveal the future predictions, and $z = 0$ represents the

present stage of the universe, we obtain the Hubble parameter $H(z)$ and deceleration parameter $q(z)$ as

$$H(z) = \frac{1}{\sqrt{3}}\sqrt{k^2(1+z)^3 + \frac{k_2 + \lambda k_4}{2(1+\lambda)}} \tag{23}$$

$$q(z) = -1 + \frac{3}{2}\frac{k^2(1+z)^3}{k^2(1+z)^3 + \frac{k_2 + \lambda k_4}{2(1+\lambda)}}. \tag{24}$$

Now we'll talk about two more geometrical parameters, which were suggested in [71]. They are called statefinder parameters r and s, and they show how the universe's geometry has changed over time and the different stages of dark energy models [71–73]. We define these parameters in terms of a scale factor.

$$r = \frac{\dddot{a}}{aH^3}, \quad s = \frac{r-1}{3(q-\frac{1}{2})} \tag{25}$$

Using the scale factor (20) in (25), we obtain the statefinder diagnostic parameters $r(t)$ and $s(t)$ as below.

$$r(t) = 1 - 3\,sech^2\left(\frac{\sqrt{3n_1}}{2}t\right) \tag{26}$$

$$s(t) = \frac{2\,sech^2\left(\frac{\sqrt{3n_1}}{2}t\right)}{3\left[1 - sech^2\left(\frac{\sqrt{3n_1}}{2}t\right)\right]} \tag{27}$$

Now we define the effective equation of state (EoS) parameter ω_{eff} by comparing the Eqs. (15) and (16) to the standard Friedmann equations in a flat spacetime universe, as

$$\omega_{eff} = \frac{p_{eff}}{\rho_{eff}} \tag{28}$$

or

$$\omega_{eff} = -1 + \frac{2n_1(\kappa^2\rho_{m0} - \lambda k^2)}{2n_1(\kappa^2\rho_{m0} - \lambda k^2) + (k_2 + \lambda k_4 - 2n_1\lambda)k^2 \sinh^2\left(\frac{\sqrt{3n_1}}{2}t\right)}. \tag{29}$$

Also, from Eq. (15), we can derive the total energy density parameter as

$$\Omega_m + \Omega_F = 1, \tag{30}$$

where

$$\Omega_m = \frac{\kappa^2\rho_m}{3H^2}, \quad \Omega_F = \frac{k_2 + \lambda k_4}{6H^2} - \lambda. \tag{31}$$

The matter energy density parameter Ω_m and the dark energy density parameter Ω_F are named respectively due to the gravity function $F(R, T)$.

In the field Eqs. (15) and (16), for $\lambda = 0$, one can obtain Einstein's field equations in GR with cosmological constant as $\Lambda = \frac{k_2}{2}$. And in this case, $\Omega_F = \frac{k_2}{6H^2} = \frac{\Lambda}{3H^2} = \Omega_\Lambda$. Also, for $\lambda \neq 0$, we can obtain varying Λ-term as a function of Hubble parameter H, as $\Lambda(H) = \frac{1}{2}(k_2 - 6\lambda H^2)$.

3.2 Model-II

In this model, we choose $u = k_1(\dot{H} + H^2) - k_2$ and $v = k_3 aH - k_4$ with k_i's $i = 1, 2, 3, 4$ constants, and $\dot{H} + H^2 = \frac{\ddot{a}}{a}$. In Eqs. (12) and (13), we obtain the following simplified field equations:

$$\frac{3}{2}(2 + 2\lambda + k_1)H^2 - \frac{1}{2}(k_2 + \lambda k_4) = \kappa^2 \rho_m \quad (32)$$

$$\frac{1}{3}(3 + k_1 + 3\lambda)(2\dot{H} + 3H^2) - \frac{1}{2}(k_2 + \lambda k_4) = -\kappa^2 p_m \quad (33)$$

Taking the non-relativistic matter pressure $p_m \approx 0$ in Eq. (33), we rewrite it as

$$2\frac{\ddot{a}}{a} + \left(\frac{\dot{a}}{a}\right)^2 - \frac{3(k_2 + \lambda k_4)}{2(3 + k_1 + 3\lambda)} = 0 \quad (34)$$

Solving Eq. (34) for scale factor $a(t)$, we get

$$a(t) = \left[\frac{3\sqrt{3}c_4 e^{\frac{\sqrt{3n_2}}{2}t} - \sqrt{3}c_3 e^{-\frac{\sqrt{3n_2}}{2}t}}{6\sqrt{n_2}}\right]^{\frac{2}{3}}, \quad n_2 > 0 \quad (35)$$

where c_3, c_4 are arbitrary constants and $n_2 = \frac{3(k_2 + \lambda k_4)}{2(3 + k_1 + 3\lambda)}$. Without loss of generality, we choose $c_3 = k\sqrt{3}$, $c_4 = \frac{k}{\sqrt{3}}$ so that we can write the scale factor as the hyperbolic expansion law.

$$a(t) = \left[\frac{k}{\sqrt{n_2}} \sinh\left(\frac{\sqrt{3n_2}}{2}t\right)\right]^{\frac{2}{3}} \quad (36)$$

Using this scale factor as in Eq. (36), we derive the Hubble parameter $H(t)$ and deceleration parameter $q(t)$ as given below:

$$H(t) = \sqrt{\frac{n_2}{3}} \coth\left(\frac{\sqrt{3n_2}}{2}t\right) \quad (37)$$

$$q(t) = -1 + \frac{3}{2}\operatorname{sech}^2\left(\frac{\sqrt{3n_2}}{2}t\right) \quad (38)$$

Again, we can express these in terms of redshift z as

$$H(z) = \frac{1}{\sqrt{3}}\sqrt{k^2(1 + z)^3 + \frac{3(k_2 + \lambda k_4)}{2(3 + k_1 + 3\lambda)}} \quad (39)$$

$$q(z) = -1 + \frac{3}{2}\frac{k^2(1 + z)^3}{k^2(1 + z)^3 + \frac{3(k_2 + \lambda k_4)}{2(3 + k_1 + 3\lambda)}} \quad (40)$$

In model II, we derive the statefinder diagnostic parameters $r(t)$ and $s(t)$.

$$r(t) = 1 - 3\operatorname{sech}^2\left(\frac{\sqrt{3n_2}}{2}t\right) \quad (41)$$

$$s(t) = \frac{2\operatorname{sech}^2\left(\frac{\sqrt{3n_2}}{2}t\right)}{3\left[1 - \operatorname{sech}^2\left(\frac{\sqrt{3n_2}}{2}t\right)\right]} \quad (42)$$

For model II, we derive the effective EoS parameter as

$$\omega_{eff} = -1 + \frac{3n_2(2\kappa^2\rho_{m0} - k_1 k^2 - 2\lambda k^2) - n_2 k_1 k^2 \sinh^2\left(\frac{\sqrt{3n_2}}{2}t\right)}{3n_2(2\kappa^2\rho_{m0} - k_1 k^2 - 2\lambda k^2) - 3k^2(2n_2\lambda + n_2 k_1 - k_2 - k_4\lambda)\sinh^2\left(\frac{\sqrt{3n_2}}{2}t\right)} \quad (43)$$

Also, from Eq. (32), we can derive the total energy density parameter for model II, as

$$\Omega_m + \Omega_F = 1, \quad (44)$$

where

$$\Omega_m = \frac{\kappa^2 \rho_m}{3H^2}, \quad \Omega_F = \frac{k_2 + \lambda k_4}{6H^2} - \lambda - \frac{1}{2}k_1. \quad (45)$$

Now, we can find the original Einstein's field equations with cosmological constant Λ-term in GR by substituting $\lambda = 0$, $k_1 = 0$, with $\Lambda = \frac{k_2}{2}$ otherwise $\Lambda(H) = \frac{1}{2}[k_2 - (3k_1 + 6\lambda)H^2]$.

4 Observational constraints

In this section, we make observational constraints on the model parameters with observational datasets in our derived model. For this, we use the freely available emcee program at [74] to perform an MCMC (Monte Carlo Markov Chain) analysis so that we can compare our derived model with observational datasets. To limit the cosmological and model parameters, the MCMC sampler changes the parameter values in a likely range of priors and looks at the parameter space posteriors. In this section, we evaluate the compatibility of the solution in the model with the cosmic chronometer (CC) data and the Pantheon datasets. These datasets pertain to the observed cosmos during a recent period.

4.1 Hubble datasets $H(z)$

For both theoretical and observational cosmologists, the Hubble parameter is one of the most important cosmological parameters for studying the evolution of the universe. It is possible to find observed values for Hubble datasets $H(z)$ with redshift z. In order to find the best values for model parameters with error bars in the redshift range $0.07 \leq z \leq 1.965$, we first use the Monte Carlo Markov Chain (MCMC) simulation to compare our derived Hubble function from the

field equations with the observed values of the 31 cosmic chronometer data points (Hubble data) [75,76]. These values were found using the differential ages (DA) of galaxies method. We can get a rough idea of the model parameters H_0, Ω_{m0}, and λ by minimizing the χ^2 function, which is the same thing as maximizing the likelihood function and is written as

$$\chi^2_{CC}(\phi) = \sum_{i=1}^{i=N} \frac{[H_{ob}(z_i) - H_{th}(\phi, z_i)]^2}{\sigma^2_{H(z_i)}},$$

where N denotes the total amount of data, H_{ob}, H_{th}, respectively, the observed and hypothesized datasets of $H(z)$ and standard deviations are displayed by $\sigma_{H(z_i)}$. Here $\phi = (H_0, \Omega_{m0}, \lambda)$.

In order to calibrate the CC datasets, we utilize Bayesian statistical analysis for Markov chain Monte Carlo (MCMC) simulation. To accomplish this, we utilize the emcee package developed by Foreman-Mackey et al. [74]. We have minimized the chi-squared statistic, $\chi^2_{CC}(\phi)$, to determine the optimal values for the model's parameters. Table 1 presents these values.

As we can see in Figs. 1 and 2, the contour plots of Model-I and Model-II show how the model parameters compare to Hubble datasets (H(z)) using MCMC analysis. We got the best fit values for the model parameters H_0, Ω_{m0}, λ by using different parameter values in the range (40, 100), (0, 1), and (0, 0.7), with confidence levels of $1 - \sigma$ and $2 - \sigma$, respectively. Table 1 lists the best fit values for each model separately. We have estimated the best fit values of model parameter $\lambda = 0.14^{+0.49}_{-0.25}, 0.38^{+0.26}_{-0.16}$ with $\Omega_{m0} = 0.38 \pm 0.15, 0.459^{+0.096}_{-0.12}$ for Model-I and Model-II, respectively. Recently, [55] estimated the value of λ as $\lambda = 0.491^{+0.387}_{-0.533}, 0.537^{+0.403}_{-0.550}$ with $\Omega_{m0} = 0.425^{+0.107}_{-0.146}, 0.339^{+0.093}_{-0.122}$, respectively, in two different models. We have estimated the value of the Hubble constant as $H_0 = 67.4 \pm 3.1, 67.8 \pm 2.9$ Km/s/Mpc, respectively, for two models, Model-I and Model-II, along CC datasets. Recently, the value of the Hubble constant was measured as $H_0 = 69.8 \pm 1.3$ Km s^{-1} Mpc^{-1} in [77], and in [78], it was measured as $H_0 = 69.7 \pm 1.2$ Km s^{-1} Mpc^{-1}. Recently, we measured the value of H_0 as $H_0 = 68.3721 \pm 1.7205$ Km/s/Mpc in [61], $H_0 = 68.3721 \pm 1.65678$ Km/s/Mpc in [59] and $H_0 = 71.66123 \pm 0.33061$ in [60].

We have considered the Hubble function for the ΛCDM model as $H(z) = H_0\sqrt{\Omega_{m0}(1 + z)^3 + \Omega_\Lambda}$ with $\Omega_\Lambda = 1 - \Omega_{m0}$ to compare our derived models I and II. That's Fig. 3, which shows the contour plots of H_0 and Ω_{m0} at $1 - \sigma$ and $2 - \sigma$ confidence levels in MCMC analysis of $H(z)$ datasets for ΛCDM. We have found the best fit values

Fig. 1 The contour plots of H_0, Ω_{m0}, λ at $1 - \sigma$ and $2 - \sigma$ confidence level in MCMC analysis of $H(z)$ datasets for Model-I

Fig. 2 The contour plots of $H_0, \Omega_{m0}, \lambda$ at $1-\sigma$ and $2-\sigma$ confidence level in MCMC analysis of $H(z)$ datasets for Model-II
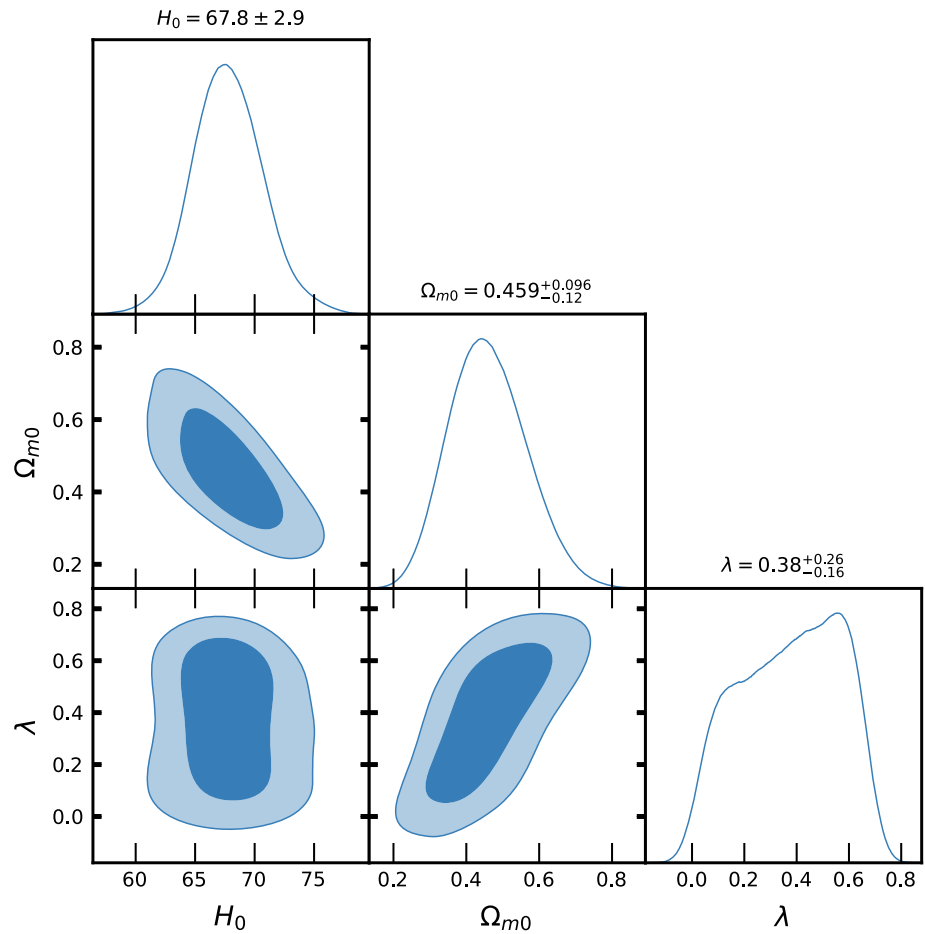
Table 1 The MCMC results in $H(z)$ datasets analysis

Parameter	Prior	Model-I	Model-II	ΛCDM
H_0	(40, 100)	67.4 ± 3.1	67.8 ± 2.9	67.7 ± 3.1
Ω_{m0}	(0, 1)	0.38 ± 0.15	$0.459^{+0.096}_{-0.12}$	$0.333^{+0.05}_{-0.07}$
λ	(0, 0.7)	$0.14^{+0.49}_{-0.25}$	$0.38^{+0.26}_{-0.16}$	–
χ^2	–	14.4936	14.4936	14.4936
χ^2_{red}	–	0.5176	0.5176	0.4998

of the Hubble constant $H_0 = 67.7 \pm 3.1$ Km/s/Mpc and the total matter energy density parameter $\Omega_{m0} = 0.333^{+0.05}_{-0.07}$, which are mentioned in Table 1. The Hubble error bar plots of 31 datasets with a best fit shape of $H(z)$ are shown in Fig. 4. These shapes were found in Models I, II, and ΛCDM, in that order.

4.2 Apparent magnitude $m(z)$

The relationship between luminosity distance and redshift is one of the main observational techniques used to track the universe's evolution. The expansion of the cosmos and the redshift of the light from distant brilliant objects are taken into consideration when calculating the luminosity distance

(D_L) in terms of the cosmic redshift (z). It is provided as

$$D_L = a_0 r (1+z), \tag{46}$$

where the radial coordinate of the source r, is established by

$$r = \int_0^r dr = \int_0^t \frac{cdt}{a(t)} = \frac{1}{a_0} \int_0^z \frac{cdz'}{H(z')}, \tag{47}$$

where we have used $dt = dz/\dot{z}, \dot{z} = -H(1+z)$.

Consequently, the following formula determines the luminosity distance:

$$D_L = c(1+z) \int_0^z \frac{dz'}{H(z')}. \tag{48}$$

Researchers widely use supernovae (SNe) as standard candles to study the cosmic expansion rate with observed apparent magnitude (m_o). The supernovae surveys that found different types of supernovae at different sizes led to the Pantheon sample SNe data set, which has 1048 data points in the range $0.01 \leq z \leq 2.26$. The theoretical apparent magnitude (m) of these standard candles is defined as [79]

$$m(z) = M + 5 \log_{10} \left(\frac{D_L}{Mpc} \right) + 25. \tag{49}$$

where M is the absolute magnitude. The luminosity distance is measured in terms of length. Based on D_L, the Hubble-
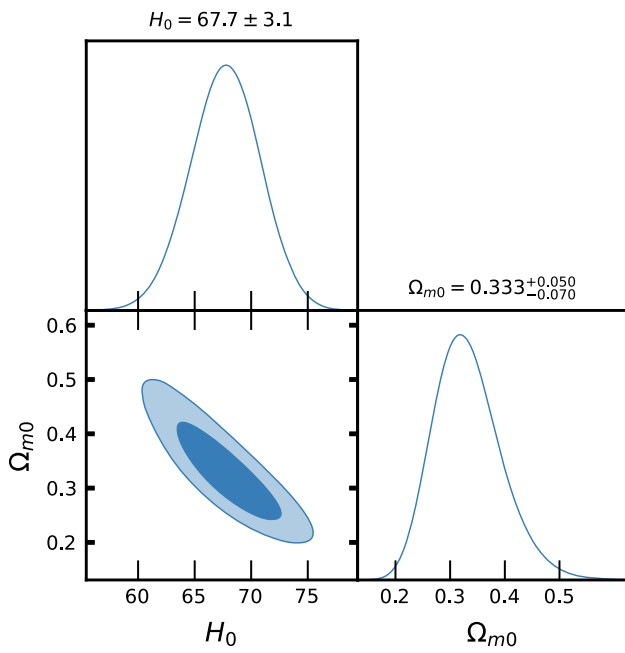
Fig. 3 The contour plot of H_0 and Ω_{m0} at $1-\sigma$ and $2-\sigma$ confidence level in MCMC analysis of $H(z)$ datasets for ΛCDM
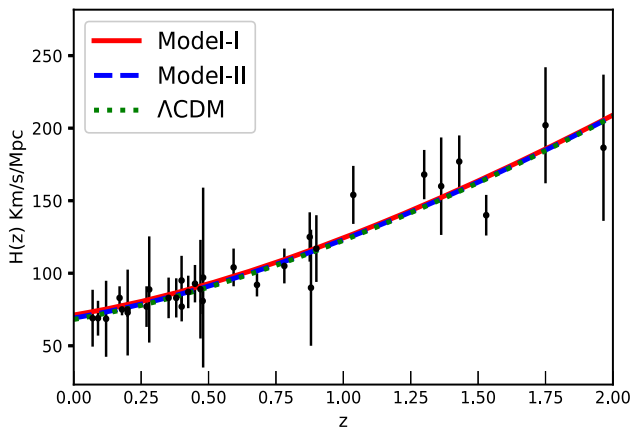
Fig. 4 The Hubble error bar plots of $H(z)$ datasets (CC datasets) over z, respectively for Model-I, Model-II and ΛCDM

free luminosity distance (d_L) may be written as $d_L \equiv \frac{H_0}{c} D_L$, which is a dimensionless quantity. Thus, we can simplify $m(z)$ as given below

$$m(z) = M + 5 \log_{10} d_L + 5 \log_{10} \left(\frac{c/H_0}{Mpc} \right) + 25. \qquad (50)$$

The degeneracy between M and H_0 may be observed using the equation above, and it is constant in the ΛCDM background [79,80]. Redefinition allows us to merge these degenerate parameters.

$$\mathcal{M} \equiv M + 5 \log_{10} \left(\frac{c/H_0}{Mpc} \right) + 25. \qquad (51)$$

The dimensionless parameter $\mathcal{M}$ can be expressed as $\mathcal{M} = M - 5 \log_{10}(h) + 42.39$, where $H_0 = h \times 100$ Km/s/Mpc. In the Markov Chain Monte Carlo (MCMC) analysis, we employ this parameter along with the corresponding χ^2 value for the Pantheon data, as given in [80].

$$\chi_P^2 = V_P^i C_{ij}^{-1} V_P^j$$

The expression V_P^i is defined as the difference between $m_o(z_i)$ and $m(z)$. The matrix C_{ij} is the inverse of the covariance matrix, and the value of $m(z)$ is determined by Eq. (14).

Figures 5 and 6 show the contour plots of model parameters for Model-I and Model-II, respectively. The Pantheon SNe Ia datasets, analyzed using MCMC, display the apparent magnitude $m(z)$. We found the best values for the model parameters $\mathcal{M}, \Omega_{m0}, \lambda$ by using values in the range (23, 24) for $\mathcal{M}$, (0, 1) for Ω_{m0}, and (0, 0.7) for λ, with confidence levels of $1-\sigma$ and $2-\sigma$. Table 2 lists the best fit values for various model parameters in each of the two models. We have estimated the best fit values of model parameter $\lambda = 0.47^{+0.26}_{-0.22}, 0.47^{+0.22}_{-0.20}$ for Model-I and Model-II, respectively, at a fixed value of $k_1 = 0.2$. Recently, [55] estimated the value of $\lambda = 0.491^{+0.387}_{-0.533}, 0.537^{+0.403}_{-0.550}$, respectively, in two different models. For two different models, we estimated the value of parameter $\mathcal{M} = 23.807^{+0.011}_{-0.013}, 23.811 \pm 0.010$, while for ΛCDM, it is found as $\mathcal{M} = 23.810 \pm 0.011$. Recently, [81] estimated the value of $\mathcal{M} = 23.809 \pm 0.013$. We found that Ω_{m0} fits best with the Pantheon SNe Ia datasets for ΛCDM. In the MCMC analysis of the Pantheon SNe Ia datasets for Lambda CDM, the best fit value for the total matter energy density parameter is currently $\Omega_{m0} = 0.300 \pm 0.021$ at $1-\sigma$ and $2-\sigma$ confidence levels (Fig. 7). Figure 8 shows the apparent magnitude error bar plots with the best fit shape of $m(z)$ derived for the models I, II, and ΛCDM.

5 Result and discussion

We can relate our fitted parameters with derived dimensionless model parameters for model-I as $k^2 = \frac{3\Omega_{m0}H_0^2}{1+\lambda}$ and $k_2 + \lambda k_4 = 6(1 + \lambda - \Omega_{m0})H_0^2$ and for model-II as $k^2 = 3H_0^2 \left[\frac{3\Omega_{m0} - \frac{1}{2}k_1}{3+k_1+3\lambda} \right]$ and $k_2 + k_4 = 6(1+\lambda+\frac{1}{2}k_1-\Omega_{m0})H_0^2$. In this paper, we solved the modified field equations for two different cases of u and v in the dust fluid source and found two exact solutions in the form of scale factor $a(t)$, called model-I and model-II. We have found a hyperbolic solution in each case (see (20) and (36)). The scale factor $a(t)$ is the most useful parameter to explore the various properties of an expanding universe, and it is a dimensionless parameter. For the estimated values of model parameters along CC datasets, we have plotted the variation of scale factor over the cosmic time t (measured in $\times 978$ Gyrs), which is

shown in Fig. 9a for models I, II, and ΛCDM model. It can be observed that $a(t)$ is an increasing function of cosmic time t, and as $t \to t_0$ (present time), then $a(t) \to 1$ (i.e., $a(t_0)$). Using this technique, we can estimate the present age of the universe as $0 \le t \le t_0$ from Fig. 9a by estimating the cosmic time t_0 at which $a(t_0) = 1$. Therefore, we have found the present age of the universe for both derived universe models, respectively, as $t_0 = 13.58^{+1.70}_{-0.51}$ Gyrs for model-I and $t_0 = 13.98^{+1.51}_{-0.72}$ Gyrs for model-II, while for ΛCDM model, it is found as $t_0 = 13.52 \pm 1.61$ Gyrs. In general, the present age of the universe can be expressed as $t_0 = 978 \times \sqrt{\frac{8(1+\lambda)}{3(k_2+\lambda k_4)}} \times \sinh^{-1}\left(k\sqrt{\frac{k_2+\lambda k_4}{2k^2(1+\lambda)}}\right)$ Gyrs. Moreover, one can find from the derived scale factor $a(t)$ that as $t \to \infty$, then $a(t) \to \infty$ in the future universe.

A dimensionless parameter $q(t)$, which is called the deceleration parameter, changes over time. This parameter can be found by figuring out the scale factor $a(t)$. This is because the deceleration parameter is defined as $q(t) = -\frac{a\ddot{a}}{\dot{a}^2}$. Equation (22) or (24) denotes the deceleration parameter (DP) for the model-I, and Eq. (38) or (40) denotes DP for the model-II. The geometrical evolution of the DP $q(z)$ for both models with ΛCDM model is depicted in Fig. 9b. From Fig. 9b, one can observe that $q(z)$ is an increasing function of redshift z and through the evolution, it shows a signature-flipping

(decelerating to accelerating) point for both models. The present value of DP is measured at $t = t_0$ or at $z = 0$ as $q_0 = -0.50^{+0.0122}_{-0.1123}$ for the model-I and $q_0 = -0.5586^{+0.0171}_{-0.0851}$ for model II, while for ΛCDM model, it is found as $q_0 = -0.5005^{+0.1750}_{-0.1050}$, which indicates our derived models are in the accelerating phase of expansion at present (at $z = 0$). This picture (Fig. 9b) also shows that as $z \to -1$, $q \to -1$ (late-time acceleration) and as $z \to \infty$, $q \to 0.5$ (early decelerating phase of an expanding universe) are both taken into account. These models are unable to explain the early accelerating (inflation) scenario of the universe's evolution. The redshift at which the deceleration parameter $q(z)$ vanishes is called the transition redshift, and it is denoted by z_t. The transition redshift is estimated as $z_t = 0.5874^{+0.2130}_{-0.0197}$ for the model-I and $z_t = 0.6865^{+0.1719}_{-0.0303}$ for the model-II, while for the ΛCDM, it is found as $z_t = 0.5882 \pm 0.1881$. The redshift z is dimensionless quantity. In general, one can derive the z_t from the expression of the deceleration parameter $q(z)$ for models I and II, as
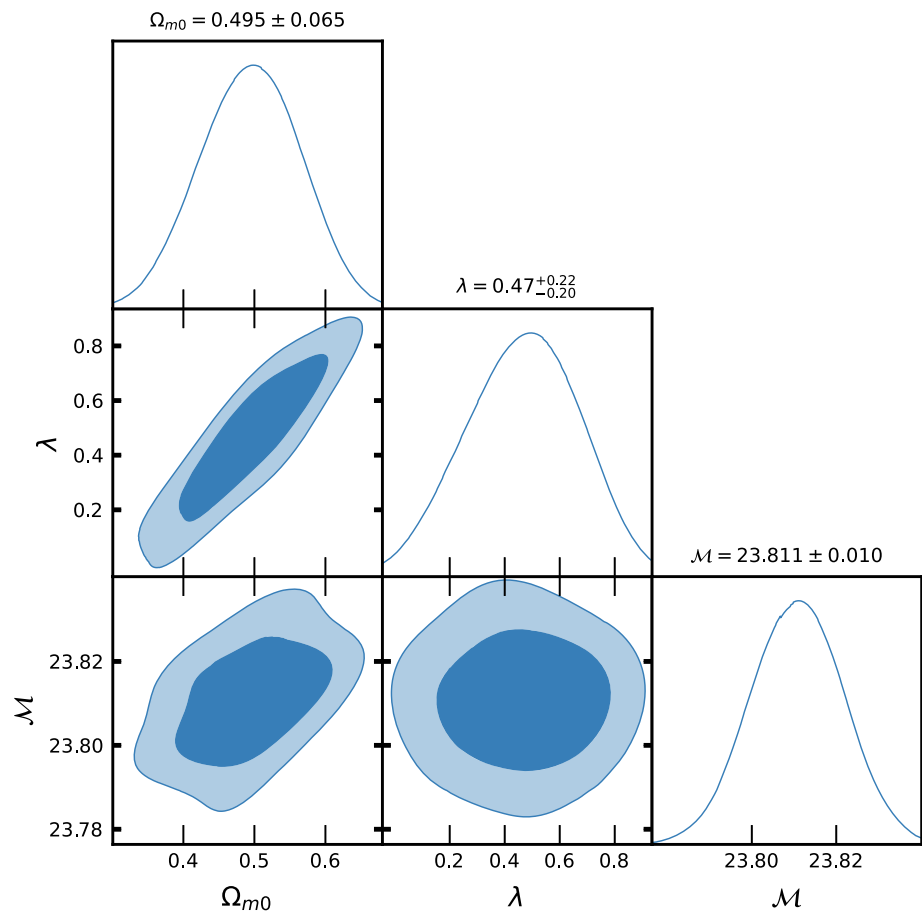
$$z_t = \left[\frac{k_2 + \lambda k_4}{k^2(1+\lambda)}\right]^{\frac{1}{3}} - 1, \quad \text{and}$$

$$z_t = \left[\frac{3(k_2 + \lambda k_4)}{k^2(3 + k_1 + 3\lambda)}\right]^{\frac{1}{3}} - 1. \quad \lambda \neq -1. \tag{52}$$

Fig. 5 The contour plot of H_0, Ω_{m0} and λ at $1-\sigma$ and $2-\sigma$ confidence level in MCMC analysis of Pantheon SNe Ia datasets for Model-I
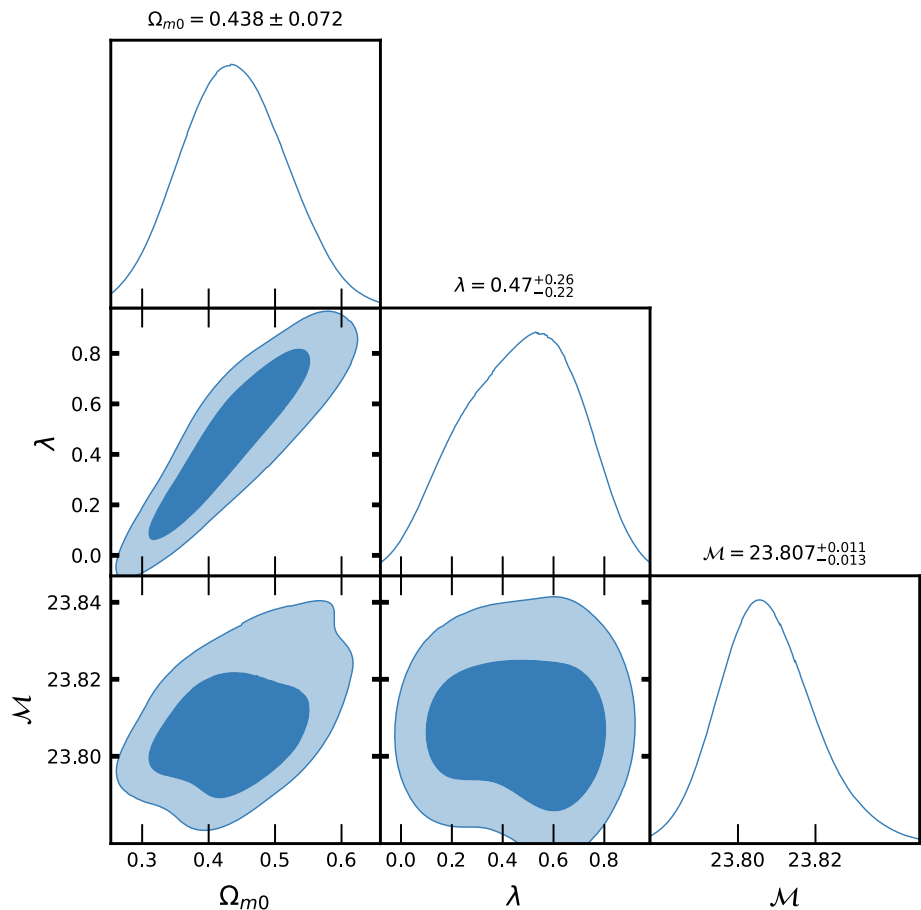
Fig. 6 The contour plot of H_0, Ω_{m0} and λ at $1 - \sigma$ and $2 - \sigma$ confidence level in MCMC analysis of Pantheon SNe Ia datasets for Model-II


**Table 2** The MCMC results in Pantheon SNe Ia datasets analysis

Parameter	Prior	Model-I	Model-II	ΛCDM
$\mathcal{M}$	(23, 24)	$23.807^{+0.011}_{-0.013}$	23.811 ± 0.010	23.810 ± 0.011
Ω_{m0}	(0, 1)	0.438 ± 0.072	0.495 ± 0.065	0.300 ± 0.021
λ	(0, 0.7)	$0.47^{+0.26}_{-0.22}$	$0.47^{+0.22}_{-0.20}$	–
χ^2	–	1026.6706	1026.6706	1026.6706
χ^2_{red}	–	0.9825	0.9825	0.9815

For the ΛCDM model, the general value of the transition redshift is found as $z_t = (2\Omega_{\Lambda 0}/\Omega_{m0})^{1/3} - 1 \approx 0.6$. This transition value shows that the universe model is in a decelerating phase of expansion for $z > z_t$ and the model is in an accelerating phase of expansion for $z < z_t$. Recently, this transition redshift $z_t = 0.74 \pm 0.05$ was obtained in [82], and in [83] it was measured as $z_t = 0.74 \pm 0.04$. In [84], this transition redshift is obtained as $z_t = 0.72 \pm 0.05$, and in 2018, [85] has suggested that the transition redshift varies over $0.33 < z_t < 1.0$. Recently, we have found this transition redshift $z_t \approx 0.7$ in [86,87]. Thus, the transition redshift $z_t = 0.5874^{+0.2130}_{-0.0197}, 0.6865^{+0.1719}_{-0.0303}$ obtained in our derived model is in good agreement with recent observed values in [82–87].
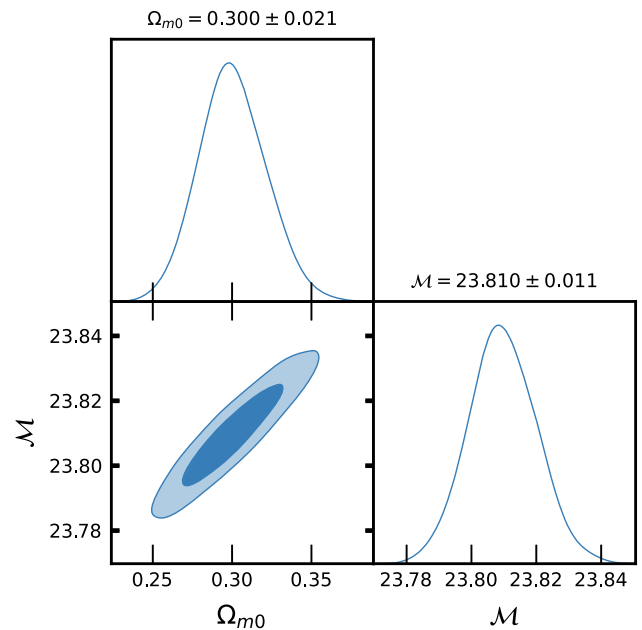
Fig. 7 The contour plot of H_0 and Ω_{m0} at $1 - \sigma$ and $2 - \sigma$ confidence level in MCMC analysis of Pantheon SNe Ia datasets for ΛCDM

The dimensionless, energy density parameters Ω_m and Ω_F are derived in Eqs. (30) and (31) for the model-I, and
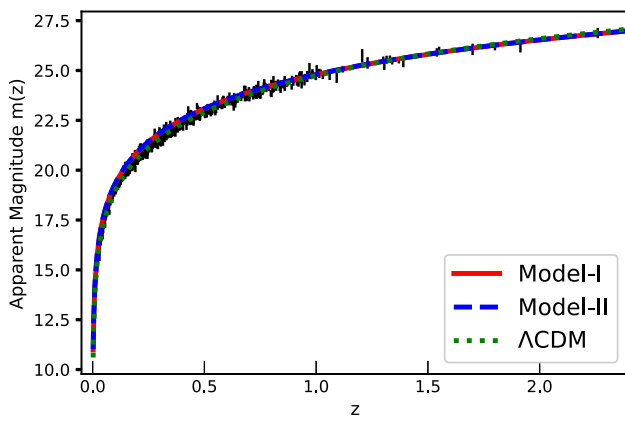
Fig. 8 The apparent magnitude error bar plots with best fit curve of $m(z)$ in the analysis of Pantheon SNe Ia datasets for the Model-I, II and ΛCDM

it is defined in Eqs. (44) and (45) for the model-II. For the flat spacetime universe, $\Omega_{m0} + \Omega_{F0} = 1$ right now. Taking this into account, we plotted the changes in Ω_m and Ω_F versus redshift z for both models with ΛCDM, which can be seen in Fig. 10a, b. From Fig. 10a, b, it can be observed that Ω_m has a decreasing nature from past to the present, while Ω_F has an increasing nature from the past to the present, which explores the past matter dominated and late-time dark energy-dominated universe scenarios. Using recent Hubble data points and Pantheon SNe Ia $m(z)$ datasets, we did a statistical analysis of the model and found that the matter energy density parameter is $\Omega_{m0} = 0.38 \pm 0.15, 0.438 \pm 0.072$ for model-I and $\Omega_{m0} = 0.459^{+0.096}_{-0.120}, 0.495 \pm 0.065$ for model-II. For the ΛCDM, it is $\Omega_{m0} = 0.333^{+0.050}_{-0.070}, 0.3 \pm 0.021$, based on two datasets, with $1-\sigma$ and $2-\sigma$ confidence level of bounds. From Fig. 10a, b, one can see that $\Omega_m \to 0$ and $\Omega_F \to 1$ as $z \to -1$ (at late-time), which reveals that our model tends to ΛCDM model at the late-time universe, and in the early universe, $\Omega_m \to 1$ and $\Omega_F \to -\lambda$ as $z \to \infty$ that shows the matter-dominated early universe.

Equations (29) and (43) represent the mathematical expressions for the dimensionless effective EoS parameter for models I and II, respectively. Figure 11a shows how ω_{eff} changes over time for both models with ΛCDM, and Fig. 11b shows how it changes over time for the matter energy density parameter ω_m. For model-I, it can be observed from Fig. 11a that $\omega_{eff} \to -1$ as $z \to -1$ (at late-time) and $\omega_{eff} \to 0$ as $z \to \infty$ (at early universe time) support early matter dominated universes and late-time dark energy-dominated universes, while for model-II, it crosses the cosmological constant value -1 with $\omega_{eff} \to -1.0345$ as $z \to -1$ that reveals that our model of universe evolves from matter dominated to quintessence, cosmological constant, and then reached the phantom dark energy-dominated phase of the expanding universe. In Fig. 11a, we can see that at the transition line $z = z_t$, the effective EoS parameter $\omega_{eff} \approx -\frac{1}{3}$.

shows how the expanding models of the universe are moving faster. The estimated present value of the effective EoS parameter is obtained as $\omega_{eff} = -0.6667^{+0.0082}_{-0.0749}$ for model-I and $\omega_{eff} = -0.7058^{+0.0114}_{-0.0567}$ for model-II, while for ΛCDM model, it is estimated as $\omega_{eff} = -0.667^{+0.05}_{-0.07}$. The change in ω_{eff} over Ω_m is shown in Fig. 11b. Using math, we can figure out the relationship between ω_{eff} and Ω_m for model-I as $(A - B)k^2\Omega_m\omega_{eff} + B\rho_{m0}\kappa^2\omega_{eff} - Bk^2\Omega_m + B\rho_{m0}\kappa^2 = 0$, where $A = 2n_1(\kappa^2\rho_{m0} - \lambda k^2)$ and $B = (k_2 + \lambda k_4 - 2n_1\lambda)k^2$. It can also be expressed as:

$$\omega_{eff} = \frac{Bk^2\Omega_m - B\rho_{m0}\kappa^2}{(A - B)k^2\Omega_m + B\rho_{m0}\kappa^2}. \tag{53}$$

From Eq. (53) and Fig. 11b, it is clear that the EoS parameter $\omega_{eff} \to -1$ for $\Omega_m \to 0$ and $\omega_{eff} \to 0$ for $\Omega_m \to \frac{\rho_{m0}\kappa^2}{k^2}$. From the above relationship, one can obtain the radiation-dominated universe for $\Omega_m > \frac{\rho_{m0}\kappa^2}{k^2}$. For model II, this relationship of ω_{eff}-Ω_m is obtained as $(A + B)k^2\Omega_m\omega_{eff} - B\rho_{m0}\kappa^2\omega_{eff} + (B - n_2k_1k^2)k^2\Omega_m - B\rho_{m0}\kappa^2 + n_2\rho_{m0}k_1k^2\kappa^2 = 0$ where $A = 3n_2(2\kappa^2\rho_{m0} - k_1k^2 - 2\lambda k^2)$ and $B = 3k^2(2n_2\lambda + n_2k_1 - k_2 - k_4\lambda)$. It can also be expressed as

$$\omega_{eff} = \frac{B\rho_{m0}\kappa^2 - n_2\rho_{m0}k_1k^2\kappa^2 - (B - n_2k_1k^2)k^2\Omega_m}{(A + B)k^2\Omega_m - B\rho_{m0}\kappa^2} \tag{54}$$

From Eq. (54), we can obtain for $\Omega_m \to 0$, $\omega_{eff} \to -1 - \frac{k_1}{6-k_1}$, $k_1 < 6$ that gives cosmological constant value. $\omega_{eff} = -1$ for $k_1 = 0$, phantom and super-phantom values for $k_1 < 6$.

Statefinder analysis:

Now, we discuss two more geometrical dimensionless parameters derived from the scale factor $a(t)$ as the statefinder diagnostic parameters $r(t)$ and $s(t)$, which are defined by the Eq. (25). For the model-I, we have derived these parameters $r(t)$ and $s(t)$ as in Eqs. (26) and (27), respectively, while for the model-II, in Eqs. (41) and (42), respectively. We can find the relation between r and s from these equations as $3rs + 6s + 2r - 2 = 0$ for the models I and II. It can be expressed as $s = \frac{2(1-r)}{3(2+r)}$, which shows that $s \to \infty$ for $r \to -2$ (singular point) and $s \to 0$ for $r \to 1$. From Eqs. (22) and (26), we can find the relationship between r & q as $r + 2q + 1 = 0$ for the models. Also, we can rewrite it as $q = -\frac{1+r}{2}$, which gives $q > 0$ for $r < -1$ and $q < 0$ for $r > -1$, and the model undergoes a transition point at $r = -1$.
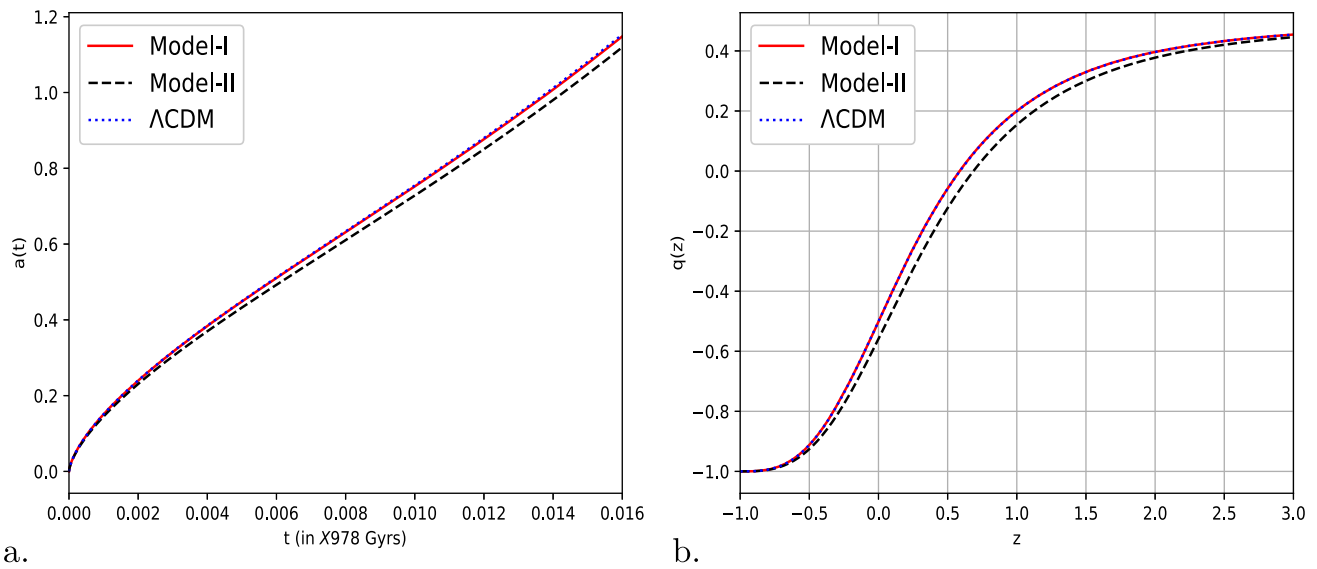
Fig. 9 Variation of scale factor over cosmic time t, and deceleration parameter $q(z)$ over z, respectively
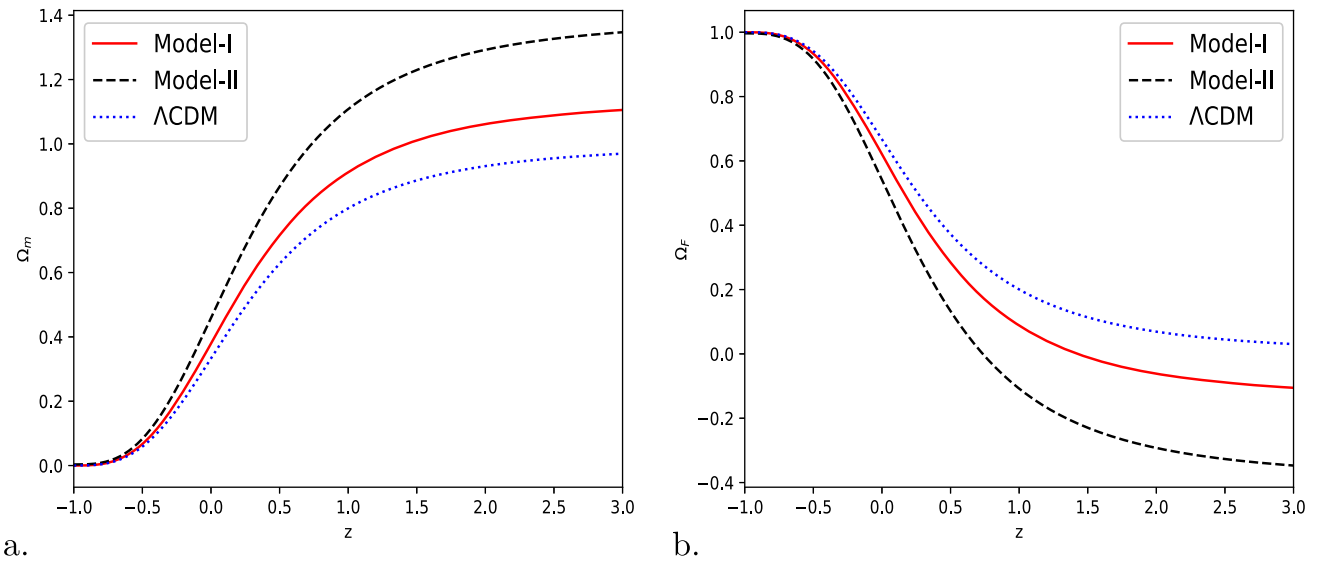
Fig. 10 The plot of total energy density parameters Ω_m and Ω_F over redshift z, respectively

Statistical analysis

In this section, we analyze different cosmological models using the Akaike information criterion (AIC) and the Bayesian information criterion (BIC). In addition, we derive the reduced chi-squared value using the formula ($\chi_{red}^2 = \chi_{min}^2/dof$), where "dof" represents the degrees of freedom. Typically, degrees of freedom are calculated as the difference between the number of data points used and the number of fitted parameters. But we should only use χ_{min}^2/dof to explain things, since the degrees of freedom might not be clear for models that aren't linear with respect to the free parameters [88]. The AIC criterion, derived from information theory, serves as an asymptotically unbiased estimator of Kullback–Leibler information. Assuming Gaussian errors, the AIC criteria can be estimated using the formula mentioned in [89,90].

$$AIC = -2\ln(\mathcal{L}_{max}) + 2n + \frac{2n(n+1)}{N-n-1}, \tag{55}$$

where $\mathcal{L}_{max}$ represents the maximum likelihood of the dataset(s) being considered, N depicts the total number of data points used in analysis, and n is the number of fitted parameters. Maximizing the likelihood function is equivalent to minimizing the χ^2 value. For a large value of N, it is evident that this expression yields the original version of AIC, which may be approximated as $AIC \simeq -2\ln(\mathcal{L}_{max}) + 2n$. According to the discussion in [91], it is widely accepted
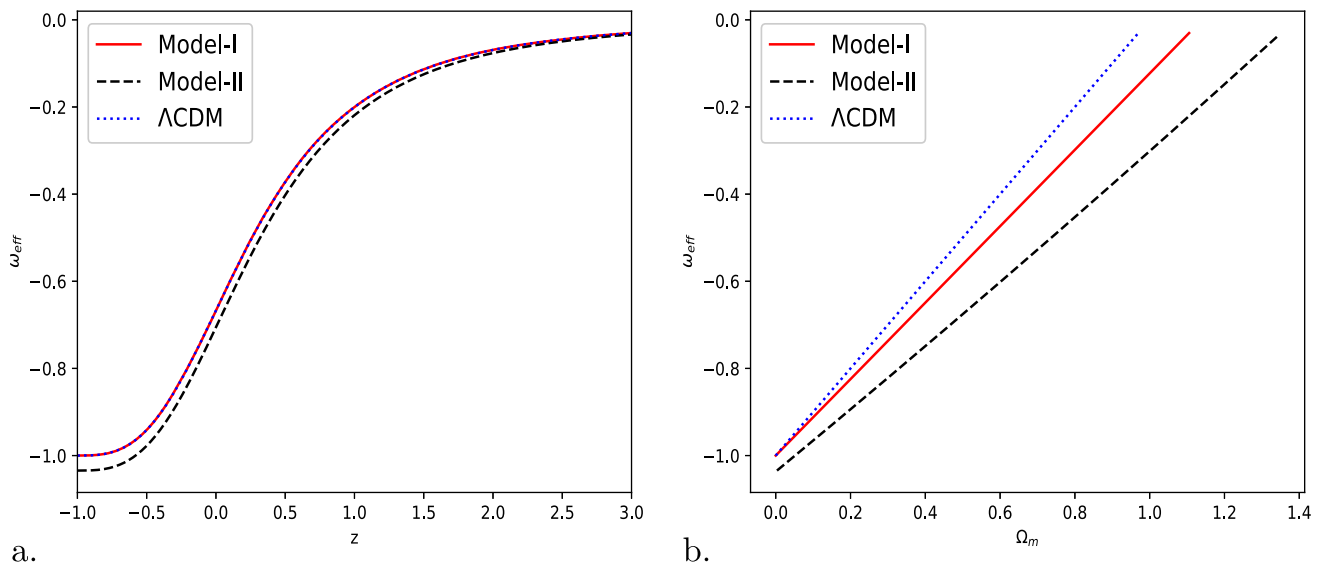
Fig. 11 The plot of effective EoS parameter ω_{eff} versus z and Ω_m, respectively

as the most effective approach to utilizing the modified AIC criterion. The BIC criteria is a Bayesian evidence estimator, and it is referenced by [89–91].

$$BIC = -2\ln(\mathcal{L}_{max}) + n\ln(N). \tag{56}$$

Our task is to arrange the models based on their ability to accurately match the available data, given a collection of scenarios that depict the same type of event. We use the two information criteria (IC) listed above to find the relative difference in the IC value for the given set of models. This is shown as $\Delta IC_{model} = IC_{model} - IC_{min}$, where IC_{min} is the model with the lowest IC value. To evaluate the suitability of each model, we utilize the Jeffreys scale [92]. More precisely, when $\Delta IC \leq 2$, it indicates that the data strongly supports the most favored model. When $2 < \Delta IC < 6$, it suggests a moderate level of disagreement between the two models. Lastly, when $\Delta IC \geq 10$, it indicates a significant level of tension between the models [47].

In our analysis, we use two types of datasets: the cosmic chronometer (Hubble data) points and the Pantheon SNe Ia datasets. By minimizing the χ^2 value, we have fitted the model parameters for our derived models, and the obtained values of χ^2_{min} and χ^2_{red} are shown in Tables 1 and 2. For models I and II, we have used $\chi^2_{min} = 14.4936$, $N = 31$, and $n = 3$ along CC datasets to obtain the AIC and BIC values, which are mentioned in the below Table 3 with the difference from the best-fitted model $\Delta IC_{model} = IC_{model} - IC_{min}$.

We used $\chi^2_{min} = 1026.6706$, $N = 1048$, and $n = 3$ to get the AIC and BIC values for the Pantheon SNe Ia datasets. The AIC and BIC values are shown below in Table 4, along with the difference from the best-fitting model, which is $\Delta IC_{model} = IC_{model} - IC_{min}$.

From the above Table 3, it is clear that both criterion AIC and BIC for both models come in the second category $2 < \Delta IC < 6$ that our derived models are less supportive of the most favored ΛCDM, while from Table 4, we can observe that the AIC criteria suggest that our derived models are less supportive of the ΛCDM model and the BIC criteria suggest strongly disagreement with the ΛCDM most favored model.

6 Conclusions

This study used a flat Friedmann–Lematre–Robertson–Walker (FLRW) spacetime metric to investigate different cosmological scenarios within the framework of metric-affine $F(R, T)$ gravity. The modified Lagrangian function being investigated is defined as $F(R, T) = R + \lambda T$, where R represents the Ricci curvature scalar, T represents the torsion scalar for the non-special connection, and λ is a parameter specific to the model. $R = R^{(LC)} + u$ and $T = T^{(W)} + v$ were used to write the equations. $R^{(LC)}$ is the Ricci scalar curvature found using the Levi-Civita connection, and $T^{(W)}$ is the torsion scalar found using the Weitzenbock connection. u and v are functions that depend on the scale factor $a(t)$, connection and its derivatives. We derived two precise solutions to the modified field equations for the scale factor $a(t)$ under two distinct scenarios of u and v. By employing this scale factor, we have derived multiple geometric parameters to examine the cosmological features of the cosmos. We used the Markov chain Monte Carlo (MCMC) simulation to look at two new sets of data: cosmic chronometer (CC) data points (Hubble data) and Pantheon SNe Ia samples. Through this analysis, we determined the model parameters that most

Table 3 The information criteria AIC and BIC for the examined cosmological models along cosmic chronometer datasets

Model	AIC	ΔAIC	BIC	ΔBIC
Model-I	21.3825	2.4603	24.7956	3.4340
Model-II	21.3825	2.4603	24.7956	3.4340
ΛCDM	18.9222	0	21.3616	0

Table 4 The information criteria AIC and BIC for the examined cosmological models, along Pantheon SNe Ia datasets

Model	AIC	ΔAIC	BIC	ΔBIC
Model-I	1032.6936	2.0115	1047.5345	6.9546
Model-II	1032.6936	2.0115	1047.5345	6.9546
ΛCDM	1030.6821	0	1040.5799	0

accurately matched the observed data within the $1 - \sigma$ and $2 - \sigma$ sectors.

We conducted a comprehensive analysis of geometric and cosmological parameters, taking into account both comparative and relativistic aspects. In model I, we have determined that the effective equation of state (EoS) parameter ω_{eff} ranges from -1 to 0, but in model II, it ranges from -1.0345 to 0. The behavior of ω_{eff} in both models reveals compatibility with the ΛCDM universe. Model-II progresses from the matter-dominated stage to the quintessence and cosmological constant stages, followed by the phantom and superphantom stages of the expanding universe. Model-I, on the other hand, moves from the matter-dominated stage to the quintessence stage, getting closer to a cosmological constant value. We have found the values of the Hubble constants $H_0 = 67.4 \pm 3.1, 67.8 \pm 2.9$ Km/s/Mpc, respectively, for the two models, while for ΛCDM $H_0 = 67.7 \pm 3.1$ Km/s/Mpc. We have determined that both models represent universes in a transitional phase, where they are transitioning from slowing down to speeding up. For these universes, the transition redshifts are $z_t = 0.5874^{+0.2130}_{-0.0197}$ and $z_t = 0.6865^{+0.1719}_{-0.0303}$, respectively. Both models show expanding universes in the transit phase, with transition redshifts between 0.3 and 1.0. We have found the present value of DP as $q_0 = -0.50^{+0.0122}_{-0.1123}$ for model I and $q_0 = -0.5586^{+0.0171}_{-0.0851}$ for model II, while for ΛCDM model, it is found as $q_0 = -0.5005^{+0.1750}_{-0.1050}$, which indicates our derived models are in the accelerating phase of expansion at present (at $z = 0$). The current values of $q(z)$ range from -0.6 to -0.5, which is in good agreement with recent observations [1–7]. Both models can explain the late-time accelerating and early decelerating scenarios of the universe, but they cannot explain the early-time accelerating (inflation) scenario of the universe. This fits well with recent measurements [82,87]. Additionally, the present age of these universes is $t_0 = 13.58^{+1.70}_{-0.51}$ Gyrs and $t_0 = 13.98^{+1.51}_{-0.72}$ Gyrs, respectively. These findings align with our current understanding of recent universes. Furthermore, we have conducted an analysis of cosmological models obtained using the AIC and BIC information criteria. This analysis aims

to assess the compatibility of our derived models with the findings of the most favored model, namely ΛCDM. Finally, from the information criterion AIC and BIC analyses of the models, we have found that our derived models are very close to ΛCDM.

Also, we have found that the dimensionless constants k_1, k_2, k_3, and k_4 are not all vanishing together, which confirms the need for investigation of such theories in this context. Thus, we can conclude that the choice of non-special connection (i.e., the choice of u and v) plays an important role in the universe's dynamical dark energy evolution history. As a result, it requires further investigation, which entices cosmologists to review it.

Data Availability Statement This manuscript has no associated data or the data will not be deposited. [Authors' comment: Data sharing not applicable to this article as no datasets were generated or analysed during the current study].

Code Availability Statement My manuscript has no associated code/software. [Authors' comment: Code/Software sharing not applicable to this article as no code/software was generated or analysed during the current study].

Declarations

Conflict of interest The author of this article has no conflict of interests. The author have no competing interests to declare that are relevant to the content of this article. Authors have mentioned clearly all received support from the organization for the submitted work.

References

1. A.G. Riess et al., Observational evidence from supernovae for an accelerating universe and a cosmological constant. Astron. J. **116**, 1009 (1998)

2. S. Perlmutter et al., Measurements of omega and lambda from 42 high-redshift supernovae. Astrophys. J. **517**, 565 (1999)

3. A.G. Riess et al., Type-Ia supernova discoveries of $z \geq 1$ from the Hubble space telescope: evidence from past deceleration and constraints on dark energy evolution. Astrophys. J. **607**, 665 (2004)

4. D.J. Eisenstein et al., Detection of the baryon acoustic peak in the large-scale correlation function of SDSS luminous red galaxies. Astrophys. J. **633**, 560 (2005)

5. W.J. Percival et al., Baryon acoustic oscillations in the Sloan Digital Sky Survey data release 7 galaxy sample. Mon. Not. R. Astron. Soc. **401**, 2148 (2010)

6. D.N. Spergel et al., First-year Wilkinson microwave anisotropy probe (WMAP) observations: determination of cosmological parameters. Astrophys. J. Suppl. Ser. **148**, 175 (2003). arXiv:astro-ph/0302209

7. T. Koivisto, D.F. Mota, Dark energy anisotropic stress and large scale structure formation. Phys. Rev. D **73**, 083502 (2006)

8. E.J. Copeland, M. Sami, S. Tsujikawa, Dynamics of dark energy. Int. J. Mod. Phys. D **15**, 1753 (2006). arXiv:hep-th/0603057

9. Y.-F. Cai, E.N. Saridakis, M.R. Setare, J.-Q. Xia, Quintom cosmology: theoretical implications and observations. Phys. Rep. **493**, 1 (2010). arXiv:0909.2776

10. K.A. Olive, Inflation. Phys. Rep. **190**, 307 (1990)

11. N. Bartolo, E. Komatsu, S. Matarrese, A. Riotto, Non-Gaussianity from inflation: theory and observations. Phys. Rep. **402**, 103 (2004). arXiv:astro-ph/0406398

12. S. Capozziello, M. De Laurentis, Extended theories of gravity. Phys. Rep. **509**, 167 (2011). arXiv:1108.6266

13. Y.F. Cai, S. Capozziello, M. De Laurentis, E.N. Saridakis, $f(T)$ teleparallel gravity and cosmology. Rep. Prog. Phys. **79**, 106901 (2016). arXiv:1511.07586

14. P. Brax, C. van de Bruck, A.C. Davis, Brane world cosmology. Rep. Prog. Phys. **67**, 2183–2232 (2004). arXiv:hep-th/0404011

15. A. De Felice, S. Tsujikawa, $f(R)$ theories. Living Rev. Relativ. **13**, 3 (2010). arXiv:1002.4928

16. S. Nojiri, S.D. Odintsov, Unified cosmic history in modified gravity: from $F(R)$ theory to Lorentz non-invariant models. Phys. Rep. **505**, 59 (2011). arXiv:1011.0544

17. S. Nojiri, S.D. Odintsov, Modified Gauss–Bonnet theory as gravitational alternative for dark energy. Phys. Lett. B **631**, 1 (2005). arXiv:hep-th/0508049

18. A. De Felice, S. Tsujikawa, Construction of cosmologically viable $f(G)$ dark energy models. Phys. Lett. B **675**, 1 (2009). arXiv:0810.5712

19. D. Lovelock, The Einstein tensor and its generalizations. J. Math. Phys. **12**, 498 (1971)

20. N. Deruelle, L. Farina-Busto, The Lovelock gravitational field equations in cosmology. Phys. Rev. D **41**, 3696 (1990)

21. G.W. Horndeski, Second-order scalar-tensor field equations in a four-dimensional space. Int. J. Theor. Phys. **10**, 363–384 (1974)

22. A. Nicolis, R. Rattazzi, E. Trincherini, The Galileon as a local modification of gravity. Phys. Rev. D **79**, 064036 (2009). arXiv:0811.2197

23. C. Deffayet, G. Esposito-Farese, A. Vikman, Covariant Galileon. Phys. Rev. D **79**, 084003 (2009). arXiv:0901.1314

24. R. Ferraro, F. Fiorini, Modified teleparallel gravity: inflation without inflaton. Phys. Rev. D **75**, 084031 (2007). arXiv:gr-qc/0610067

25. E.V. Linder, Einstein's other gravity and the acceleration of the universe. Phys. Rev. D **81**, 127301 (2010). arXiv:1005.3039

26. G. Kofinas, E.N. Saridakis, Teleparallel equivalent of Gauss–Bonnet gravity and its modifications. Phys. Rev. D **90**, 084044 (2014). arXiv:1404.2249

27. C.-Q. Geng, C.-C. Lee, E.N. Saridakis, Y.-P. Wu, Teleparallel dark energy. Phys. Lett. B **704**, 384–387 (2011). arXiv:1109.1092

28. M. Hohmann, L. Järv, U. Ualikhanova, Covariant formulation of scalar-torsion gravity. Phys. Rev. D **97**, 104011 (2018). arXiv:1801.05786

29. R. Aldrovandi, J.G. Pereira, *Teleparallel Gravity: An Introduction* (Springer, Dordrecht, 2013)

30. J.W. Maluf, The teleparallel equivalent of general relativity. Ann. Phys. **525**, 339 (2013). arXiv:1303.3897

31. F.W. Hehl, J.D. McCrea, E.W. Mielke, Y. Ne'eman, Metric affine gauge theory of gravity: field equations, Noether identities, world spinors, and breaking of dilation invariance. Phys. Rep. **258**, 1 (1995). arXiv:gr-qc/9402012

32. J. Beltran Jimenez, A. Golovnev, M. Karciauskas, T.S. Koivisto, The bimetric variational principle for general relativity. Phys. Rev. D **86**, 084024 (2012). arXiv:1201.4018

33. N. Tamanini, Variational approach to gravitational theories with two independent connections. Phys. Rev. D **86**, 024004 (2012). arXiv:1205.2511

34. G.Y. Bogoslovsky, H.F. Goenner, Finslerian spaces possessing local relativistic symmetry. Gen. Relativ. Gravit. **31**, 1565 (1999). arXiv:gr-qc/9904081

35. N.E. Mavromatos, S. Sarkar, A. Vergou, Stringy space-time foam, Finsler-like metrics and dark matter relics. Phys. Lett. B **696**, 300 (2011). arXiv:1009.2880

36. S. Basilakos, A.P. Kouretsis, E.N. Saridakis, P. Stavrinos, Resembling dark energy and modified gravity with Finsler–Randers cosmology. Phys. Rev. D **88**, 123510 (2013). arXiv:1311.5915

37. A.P. Kouretsis, M. Stathakopoulos, P.C. Stavrinos, Covariant kinematics and gravitational bounce in Finsler space-times. Phys. Rev. D **86**, 124025 (2012). arXiv:1208.1673

38. A. Triantafyllopoulos, P.C. Stavrinos, Weak field equations and generalized FRW cosmology on the tangent Lorentz bundle. Class. Quantum Gravity **35**, 085011 (2018)

39. S. Ikeda, E.N. Saridakis, P.C. Stavrinos, A. Triantafyllopoulos, Cosmology of Lorentz fiber-bundle induced scalar-tensor theories. Phys. Rev. D **100**, 124035 (2019). arXiv:1907.10950

40. A. Conroy, T. Koivisto, The spectrum of symmetric teleparallel gravity. Eur. Phys. J. C **78**, 923 (2018). arXiv:1710.05708

41. R. Myrzakulov, FRW cosmology in $F(R, T)$ gravity. Eur. Phys. J. C **72**, 2203 (2012). arXiv:1207.1039

42. E.N. Saridakis, S. Myrzakul, K. Myrzakulov, K. Yerzhanov, Cosmological applications of $F(R, T)$ gravity with dynamical curvature and torsion. Phys. Rev. D **102**, 023525 (2020). arXiv:1912.03882

43. M. Jamil, D. Momeni, M. Raza, R. Myrzakulov, Reconstruction of some cosmological models in $f(R, T)$ gravity. Eur. Phys. J. C **72**, 1999 (2012). arXiv:1107.5807

44. M. Sharif, S. Rani, R. Myrzakulov, Analysis of $F(R, T)$ gravity models through energy conditions. Eur. Phys. J. Plus **128**, 123 (2013). arXiv:1210.2714

45. S. Capozziello, M. De Laurentis, R. Myrzakulov, Noether symmetry approach for teleparallel-curvature cosmology. Int. J. Geom. Methods Mod. Phys. **12**, 1550095 (2015). arXiv:1412.1471

46. P. Feola, X.J. Forteza, S. Capozziello, R. Cianci, S. Vignolo, The mass-radius relation for neutron stars in $f(R) = R + \alpha R^2$ grav-

ity: a comparison between purely metric and torsion formulations (2019). arXiv:1909.08847

47. F.K. Anagnostopoulos, S. Basilakos, E.N. Saridakis, Observational constraints on Myrzakulov gravity (2020). arXiv:2012.06524

48. N. Myrzakulov, R. Myrzakulov, L. Ravera, Metric-affine Myrzakulov gravity theories (2021). arXiv:2108.00957

49. D. Iosifidis, N. Myrzakulov, R. Myrzakulov, Metric-affine version of Myrzakulov $F(R, T, Q, T)$ gravity and cosmological applications. Universe **7**, 262 (2021). arXiv:2106.05083

50. T. Harko, N. Myrzakulov, R. Myrzakulov, S. Shahidi, Non-minimal geometry-matter couplings in Weyl–Cartan space-times: Myrzakulov $F(R, T, Q, T_m)$ gravity (2022). arxiv:2110.00358v1

51. R. Saleem, A. Saleem, Variable constraints on some Myrzakulov models to study Baryon asymmetry. Chin. J. Phys. **84**, 471–485 (2023)

52. D. Iosifidis, R. Myrzakulov, L. Ravera, G. Yergaliyeva, K. Yerzhanov, Metric-affine vector-tensor correspondence and implications in $F(R, T, Q, T, D)$ gravity (2021). arXiv:2111.14214

53. G. Papagiannopoulos, S. Basilakos, E.N. Saridakis, Dynamical system analysis of Myrzakulov gravity (2022). arXiv:2202.10871

54. S. Kazempour, A.R. Akbarieh, Cosmological study in $F(R, T)$ quasi-dilaton massive gravity (2023). arXiv:2309.09230

55. F.K. Anagnostopoulos, S. Basilakos, E.N. Saridakis, Observational constraints on Myrzakulov gravity. Phys. Rev. D **103**, 104013 (2021). arXiv:2012.06524 [gr-qc]

56. D.C. Maurya, R. Myrzakulov, Transit cosmological models in Myrzakulov $F(R, T)$ gravity theory (2024). arXiv:2401.00686 [gr-qc]

57. D.C. Maurya, K. Yesmakhanova, R. Myrzakulov, G. Nugmanova, FLRW cosmology in Myrzakulov $F(R, Q)$ gravity (2024). arXiv:2403.11604 [gr-qc]

58. D.C. Maurya, K. Yesmakhanova, R. Myrzakulov, G. Nugmanova, Myrzakulov $F(T, Q)$ gravity: cosmological implications and constraints (2024). arXiv:2404.09698 [gr-qc]

59. D.C. Maurya, A. Dixit, A. Pradhan, Transit string dark energy models in $f(Q)$ gravity. Inter. J. Geom. Methods Mod. Phys. **20**, 2350134 (2023)

60. D.C. Maurya, Phantom dark energy nature of string-fluid cosmological models in $f(Q)$-gravity. Gravit. Cosmol. **29**(4), 345–361 (2023)

61. D.C. Maurya, J. Singh, Modified $f(Q)$-gravity string cosmological models with observational constraints. Astron. Comput. **46**, 100789 (2024). https://doi.org/10.1016/j.ascom.2024.100789

62. D.C. Maurya, Reconstructing ΛCDM $f(T)$ gravity model with observational constraints. Int. J. Geom. Methods Mod. Phys. (2024). https://doi.org/10.1142/S0219887824500397

63. A. Dixit, A. Pradhan, D.C. Maurya, A probe of cosmological models in modified teleparallel gravity. Int. J. Geom. Methods Mod. Phys. **18**, 2150208 (2023)

64. D.C. Maurya, Accelerating scenarios of viscous fluid universe in modified $f(T)$ gravity. Int. J. Geom. Methods Mod. Phys. **19**, 2250144 (2022)

65. R. Zia, D.C. Maurya, A.K. Shukla, Transit cosmological models in modified $f(Q, T)$ gravity. Int. J. Geom. Methods Mod. Phys. **18**, 2150051 (2021)

66. F.K. Anagnostopoulos, S. Basilakos, E.N. Saridakis, First evidence that non-metricity $f(Q)$ gravity could challenge ΛCDM. Phys. Lett. B **822**, 136634 (2021). arXiv:2104.15123 [gr-qc]

67. A. De, T.-H. Loo, E.N. Saridakis, Non-metricity with bounday terms: $f(Q, C)$ gravity and cosmology. JCAP **03**, 050 (2024). arXiv:2308.00652 [gr-qc]

68. A. Paliathanasis, S. Basilakos, E.N. Saridakis, S. Capozziello, K. Atazadeh, F. Darabi, M. Tsamparlis, New Schwarzschild-like solutions in $f(T)$ gravity through Noether symmetries. Phys. Rev. D **89**, 104042 (2014). arXiv:1402.5935

69. A. Paliathanasis, $f(R)$-gravity from killing tensors. Class. Quantum Gravity **33**, 075012 (2016). arXiv:1512.03239

70. N. Dimakis, A. Karagiorgos, A. Zampeli, A. Paliathanasis, T. Christodoulakis, P.A. Terzis, General analytic solutions of scalar field cosmology with arbitrary potential. Phys. Rev. D **93**, 123518 (2016). arXiv:1604.05168

71. V. Sahni et al., Statefinder—a new geometrical diagnostic of dark energy. JETP Lett. **77**, 201 (2003)

72. U. Alam et al., Exploring the expanding universe and dark energy using the Statefinder diagnostic. Mon. Not. R. Astron. Soc. **344**, 1057 (2003)

73. M. Sami et al., Cosmological dynamics of a nonminimally coupled scalar field system and its late time cosmic relevance. Phys. Rev. D **86**, 103532 (2012)

74. D. Foreman-Mackey, D.W. Hogg, D. Lang, J. Goodman, Publ. Astron. Soc. Pac. **125**, 306 (2013). https://doi.org/10.1086/670067

75. J. Simon, L. Verde, R. Jimenez, Phys. Rev. D **71**, 123001 (2005). https://doi.org/10.1103/PhysRevD.71.123001

76. G.S. Sharov, V.O. Vasiliev, Math. Model. Geom. **6**, 1–20 (2018). https://doi.org/10.26456/mmg/2018-611

77. S. Cao, B. Ratra, $H_0 = 69.8 \pm 1.3\ km\ s^{-1}\ Mpc^{-1}$, $\Omega_{m0} = 0.288 \pm 0.017$, and other constraints from lower-redshift, non-CMB, expansion-rate data. Phys. Rev. D **107**, 103521 (2023). arXiv:2302.14203 [astro-ph.CO]

78. S. Cao, B. Ratra, Using lower-redshift, non-CMB, data to constrain the Hubble constant and other cosmological parameters. MNRAS **513**, 5686–5700 (2022). arXiv:2203.10825 [astro-ph.CO]

79. G. Ellis, R. Maartens, M. MacCallum, *Relativistic Cosmology* (Cambridge University Press, Cambridge, 2012). https://doi.org/10.1017/CBO9781139014403

80. K. Asvesta, L. Kazantzidis, L. Perivolaropoulos, C.G. Tsagas, Mon. Not. R. Astron. Soc. **513**, 2394–2406 (2022). https://doi.org/10.1093/mnras/stac922

81. A.R. Lalke, G.P. Singh, A. Singh, Cosmic dynamics with late-time constraints on the parametric deceleration parameter model. Eur. Phys. J. Plus **139**, 288 (2024). https://doi.org/10.1140/epjp/s13360-024-05091-5

82. O. Farooq, B. Ratra, Hubble parameter measurement constraints on the cosmological deceleration-acceleration transition redshift (2013). arXiv:1301.5243v1 [astro-ph.CO]

83. O. Farooq, S. Crandall, B. Ratra, Binned Hubble parameter measurements and the cosmological deceleration-acceleration transition (2013). arXiv:1305.1957v1 [astro-ph.CO]

84. O. Farooq, F. Madiyar, S. Crandall, B. Ratra, Hubble parameter measurement constraints on the redshift of the deceleration-acceleration transition, dynamical dark energy, and space curvature (2016). arXiv:1607.03537v2 [astro-ph.CO]

85. H. Yu, B. Ratra, F.-Y. Wang, Hubble parameter and baryon acoustic oscillation measurement constraints on the Hubble constant, the deviation from the spatially-flat Λcdm model. The deceleration-acceleration transition redshift, and spatial curvature (2018). arXiv:1711.03437v2 [astro-ph.CO]

86. D.C. Maurya, R. Zia, Brans–Dicke scalar field cosmological model in Lyra's geometry. Phys. Rev. D **100**(2), 023503 (2019). https://doi.org/10.1103/PhysRevD.100.023503

87. D.C. Maurya, J. Singh, L.K. Gaur, Dark energy nature in logarithmic $f(R, T)$ cosmology. Int. J. Geom. Methods Mod. Phys. **20**(11), 2350192 (2023). https://doi.org/10.1142/S021988782350192X

88. R. Andrae, T. Schulze-Hartung, P. Melchior, Dos and don'ts of reduced chi-squared. arXiv:1012.3754

89. K. Anderson, *Model Selection and Multimodel Inference: A Practical Information-theoretic Approach*, 2nd edn. (Springer, New York, 2002)

90. K.P. Burnham, D.R. Anderson, Multimodel inference: understanding AIC and BIC in model selection. Sociol. Methods Res. **33**, 261 (2004)

91. A.R. Liddle, Information criteria for astrophysical model selection. Mon. Not. R. Astron. Soc. **377**, L74 (2007). [arXiv:astro-ph/0701113]
92. R.E. Kass, A.E. Raftery, Bayes factors. J. Am. Stat. Assoc. **90**, 430–773 (1995)